Available online at www.sciencedirect.com
ScienceDirect
Ceramics International 37 (2011) 627–634
CERAMICS INTERNATIONAL
www.elsevier.com/locate/ceramint

Modelling the pressure dependence and the influence of added polymeric fibers on the permeability of refractory concretes

B. Collignon [a,b], C. Moyne [b], J.-L. Guichard [a], C. Perrot [a], Y. Jannot [b,*]

[a] ICAR, 4 rue Lavoisier 54300 Moncel les Lunéville, France
[b] LEMTA, Nancy-University, CNRS, 2 avenue de la Forêt de Haye BP160, 54504 Vandœuvre-lès-Nancy, France

Received 9 July 2010; received in revised form 16 September 2010; accepted 30 September 2010
Available online 28 October 2010

Abstract

In order to facilitate the water evacuation during drying, polymeric fibers are added to refractory concretes. A permeability model using Bruggeman's approach is developed to predict the permeability increase due to the fibers addition. This model (without adjustable parameters) knowing the fibers geometry (given by the manufacturer) and added amount (mass fraction varying between 0 and 0.20%) is validated by a thorough comparison with experimental results. The refractory permeability is measured at ambient temperature varying the quantity of added organic fibers after the samples were fired at different temperatures (from 80 °C to 500 °C). The analysis of results is especially careful to take into account the influence on the permeability, on both pressure (Klinkenberg effect) and firing temperature. The agreement between theoretical and experimental results is shown to be very satisfactory.

Keywords: Refractory; Concrete; Polymeric fibers; Permeability

1. Introduction

Permeability is an important parameter in the processing of refractory concretes. It provides information on the ability to evacuate the water content during drying. This step is crucial because it determines the lifetime of refractory concretes. Conducted in bad conditions, it can lead to an explosive spalling of the refractory corresponding to an internal gas pressure raise linked to the water saturated vapor pressure increase with temperature. In fact, low-permeability structures can retain water and in such cases, fast heating rates cause pressure buildup by vapor formation, damaging or even exploding the refractory body.

An important method to minimize the susceptibility of refractory concrete to explosive spalling is the use of drying additives. Organic polypropylene fibers may be added to the concrete composition to help water transfer. When the temperature increases, the fibers melt and create channels to facilitate water drainage.

As shown early by Bazant and Thonghutai [1], the main drying mechanism is vapor filtration with the pore vapor pressure as the driving force. The permeability of castable refractory concretes was then widely studied [2–4]. Experimental permeability data obtained with various refractory materials emphasize the discrepancy with the results obtained with Darcy's law, usually used. The permeability has then been represented either by the model of Forchheimer or Klinkenberg.

Other works have studied the influence of an addition of organic fibers on the permeability [5–8]. Analyzing experimental results, the influence of the length and the diameter of fibers on the permeability has been tested measuring the permeability both at room temperature before and after the firing of samples or also at high temperatures. The tests consist in applying a constant pressure drop through the sample and in measuring the exiting airflow, while the temperature of the sample varies. They demonstrate that the presence of fibers does not influence the permeability at low temperatures but increases it after firing.

To determine the influence of the fibers diameter on the permeability, tests were also carried out with the same

* Corresponding author.
E-mail addresses: collignon.icar@ceramique.fr (B. Collignon), Christian.Moyne@ensem.inpl-nancy.fr (C. Moyne), guichard.icar@ceramique.fr (J.L. Guichard), perrot.icar@ceramique.fr (C. Perrot), Yves.Jannot@ensem.inpl-nancy.fr (Y. Jannot).

0272-8842/$36.00
doi:10.1016/j.ceramint.2010.09.030

operating mode (constant pressure drop through the sample). Increasing the fibers diameter does not increase the value of the permeability but has rather the inverse effect. It was also noticed that increasing the diameter of fibers does not affect the permeability at low-temperature but leads to a decreasing permeability value after firing: the diameter increase at constant fiber volume fraction decreases the channels number, which is insufficient for creating an optimal network.

In this work, we first look at the definition, modeling and measurement of the gas permeability of refractory. In a second step, we study how the addition of fibers modifies the refractory permeability. Since permeability measurement at high temperature is difficult to carry on and cannot be accurate, the following experimental procedure has been chosen:

- Castable preparation with different fiber contents.
- Firing at different temperatures (from 80 °C up to 500 °C).
- Permeability measurement at 20 °C after sample cooling.

Since micro-damaging may occur in the sample during the cooling phase, the measured permeability at 20 °C may be different from the true permeability at the firing temperature. Nevertheless as the fiber content is sufficiently low to have no influence on this micro-damaging, the ratio of the permeability of the castable with fibers K_{eq} to the permeability of the castable without fiber K_0 is assumed not to be affected by the cooling phase.

The aim of this study is to quantify the permeability increasing due to the fusion of the fibers.

Some experiments are made varying both the temperature and the amount of fibers and a mathematical model predicting the influence of the fibers is developed.

2. Permeability modelling

2.1. Homogeneous porous media: Forchheimer and Klinkenberg effects

The flow of a fluid through a porous medium is generally governed by Darcy law:

$$-\frac{dP}{dx} = \frac{\mu}{K} q \tag{1}$$

where q_v is the superficial velocity, μ the dynamic viscosity and dP/dx the pressure gradient. The intrinsic permeability, proportional to the square of length, is a strictly geometrical property, dependent only on the microstructure of the material.

This general law requires a correction in the two following cases:

- High-velocity flow for a high permeability material: non-linear effects have to be taken into account resulting in the Forchheimer relation [9–11]:

$$-\frac{dP}{dx} = \frac{\mu}{K} q + \frac{\rho}{K_2} q^2 \tag{2}$$

  This correction applies for Reynolds number $Re = \rho q d_g/((1-\varepsilon)\mu)$ higher than $\approx 1-10$ where d_g is the mean grain diameter and ε the porosity.
- Gas flow in a low permeable material with small pores resulting in the Klinkenberg relation [12,13]:

$$-\frac{dP}{dx} = \frac{\mu}{K_{liq}(1+(B/P))} q \tag{3}$$

  where K_{liq} is the intrinsic liquid permeability and B is a constant value which has the dimension of a pressure. By regression on a large number of experimental results for K_{liq} and B, Jones proposes the following relation [14]:

$$B = 1.89 \times 10^{-6} K_{liq}^{-0.36} \tag{4}$$

  where the intrinsic permeability K_{liq} is in m^2 and B in bar. This relation resulting from a large number of experimental results on diverse materials can provide only a rough estimate.

2.2. Heterogeneous porous media

The objective of this section is to calculate the permeability K_{eq} of a continuous phase (“0”) of permeability K_0 in which inclusions (“1”) of permeability K_1 with a volume fraction ε_1 are added. As fibers are added randomly, the Bruggeman model [15,16] is chosen. It assumes a continuous addition of inclusions of permeability K_1 in a porous medium of permeability K_{eq}. In what follows, the inclusions are supposed to be of an ellipsoidal shape of small half-axes b and c and of larger half-axis a.

As the pressure field satisfies the Laplace equation, the pressure gradient inside an ellipsoidal inclusion of half-axes $c \le b \le a$ embedded in a matrix of permeability K_0 with a uniform pressure gradient applied at infinity is constant and given by:

$$\nabla p_1 = \zeta \nabla p_0|_\infty \quad \text{with } \zeta = \frac{1}{3}\left[\frac{1}{1+A_0((K_1/K_0)-1)} + \frac{1}{1+B_0((K_1/K_0)-1)} + \frac{1}{1+C_0((K_1/K_0)-1)}\right] \tag{5}$$

where the coefficients A_0, B_0 and C_0 (linked by $A_0 + B_0 + C_0 = 1$) are given by [17]:

$$A_0 = \frac{1}{2}abc\int_0^\infty \frac{du}{(a^2+u)^{3/2}(b^2+u)^{1/2}(c^2+u)^{1/2}}$$
$$B_0 = \frac{1}{2}abc\int_0^\infty \frac{du}{(a^2+u)^{1/2}(b^2+u)^{3/2}(c^2+u)^{1/2}} \tag{6}$$
$$C_0 = \frac{1}{2}abc\int_0^\infty \frac{du}{(a^2+u)^{1/2}(b^2+u)^{1/2}(c^2+u)^{3/2}}$$

Note that if $c \ll b \le a$,

$$\zeta \approx \frac{1}{3[1+A_0((K_1/K_{eq})-1)]} \tag{7}$$

If the particular case where the two small half-axes are equal ($b = c \le a$) (prolate ellipsoid), these coefficients are given

analytically by the following expressions:

$$A_0 = \frac{1-e^2}{e^3}\left[\frac{1}{2}\ln\left(\frac{1+e}{1-e}\right) - e\right]$$
$$B_0 = C_0 = \frac{1-e^2}{2e^3}\left[\frac{e}{1-e^2} - \frac{1}{2}\ln\left(\frac{1+e}{1-e}\right)\right] \quad (8)$$

with $e = \sqrt{1-(b^2/a^2)}$.

The pressure gradient and the Darcy flux are now averaged to give

$$_{\mathrm{D}} = -\varepsilon_0 K_0 \langle \nabla p \rangle^0 - \varepsilon_1 K_1 \langle \nabla p \rangle^1 \quad (9)$$

$$\langle \nabla p \rangle = \varepsilon_0 \langle \nabla p \rangle^0 + \varepsilon_1 \langle \nabla p \rangle^1 \quad (10)$$

where ε_0 and ε_1 are the volume fraction of the continuous phase and of the inclusions ($\varepsilon_0 + \varepsilon_1 = 1$), $\langle \nabla p \rangle^i$ is the volume averaged pressure gradient on phase i and $\langle \nabla p \rangle$ the pressure gradient averaged on the whole medium. Combining relations (9) and (10) leads to

$$_{\mathrm{D}} = -[K_0 + \varepsilon_1 (K_1 - K_0)\zeta]\langle \nabla p \rangle \quad (11)$$

where $\zeta = \langle \nabla p \rangle^1 / \langle \nabla p \rangle$ is the ratio between the average pressure gradient inside the inclusions of permeability K_1 and the averaged pressure gradient for the whole medium of permeability K_{eq} at infinity defined according to (11) by

$$K_{\mathrm{eq}} = K_0 + \varepsilon_1 (K_1 - K_0)\zeta \quad (12)$$

In the Bruggeman model, the inclusions are progressively added to the continuous phase "0". To vary the inclusion volume fraction of $\Delta\varepsilon_1$, it is therefore necessary to add a quantity of inclusions $\Delta\varepsilon_1/(1-\varepsilon_1)$ to the continuous phase. Then:

$$K_{\mathrm{eq}}(\varepsilon_1 + \Delta\varepsilon_1) = K_{\mathrm{eq}}(\varepsilon_1) + \frac{\Delta\varepsilon_1}{1-\varepsilon_1}(K_1 - K_{\mathrm{eq}})\zeta \quad (13)$$

or

$$dK_{\mathrm{eq}} = \frac{d\varepsilon_1}{1-\varepsilon_1}(K_1 - K_{\mathrm{eq}})\zeta \quad (14)$$

After integration and using relation (7), the final result is obtained

$$\left(\frac{K_{\mathrm{eq}}}{K_0}\right)^{A_0}\left(\frac{K_1 - K_0}{K_1 - K_{\mathrm{eq}}}\right) = (1-\varepsilon_1)^{-1/3} \quad (15)$$

The permeability of the holes left by the fibers melting is essential in the direction of the fibers length L_{f}. In the transverse directions, it is reasonable to assume that the permeability is still larger. As this transverse permeability plays no role on the permeability of the whole medium as the volume fraction occupied by fibers is very low, the holes permeability is assumed to be isotropic with a value equal to the longitudinal permeability. The longitudinal permeability is determined by assuming a Poiseuille flow with a no-slip condition at the fibers surface. Therefore [18]:

$$K_1 = \frac{b^2 c^2}{4(b^2 + c^2)} \quad (16)$$

If $b = c$, notice that $K_1 = b^2/8$.

When $K_{\mathrm{eq}}/K_1 \ll \varepsilon_1/3$, formula (15) becomes:

$$\frac{K_{\mathrm{eq}}}{K_0} = \exp\left(\frac{\varepsilon_1}{3A_0}\right) \quad (17)$$

2.3. Effect of fiber length and diameter

In this section, the influence of the length L_{f} and of the diameter d_{f} of the fibers on the equivalent permeability K_{eq} is studied. The fibers volume fraction is $\varepsilon_{\mathrm{f}} = 0.34$ % (this corresponds to a mass fraction $\omega_{\mathrm{f}} = 0.10$ %). The permeability of the continuous phase is $K_0 = 10^{-16}$ m^2. The individualized cylindrical fibers are seen as elongated ellipsoids of length $2a = L_{\mathrm{f}}$ and of equal small half-axes $b = c$ such as the volume of the fiber is preserved (Fig. 1).

Fig. 2 represents the influence of the length of fibers on the equivalent permeability (divided by the continuous phase permeability) for the Bruggeman model (($d_{\mathrm{f}} = 15$ μm)). For a given volume fraction ε_{f} and a given fibers diameter d_{f}, the

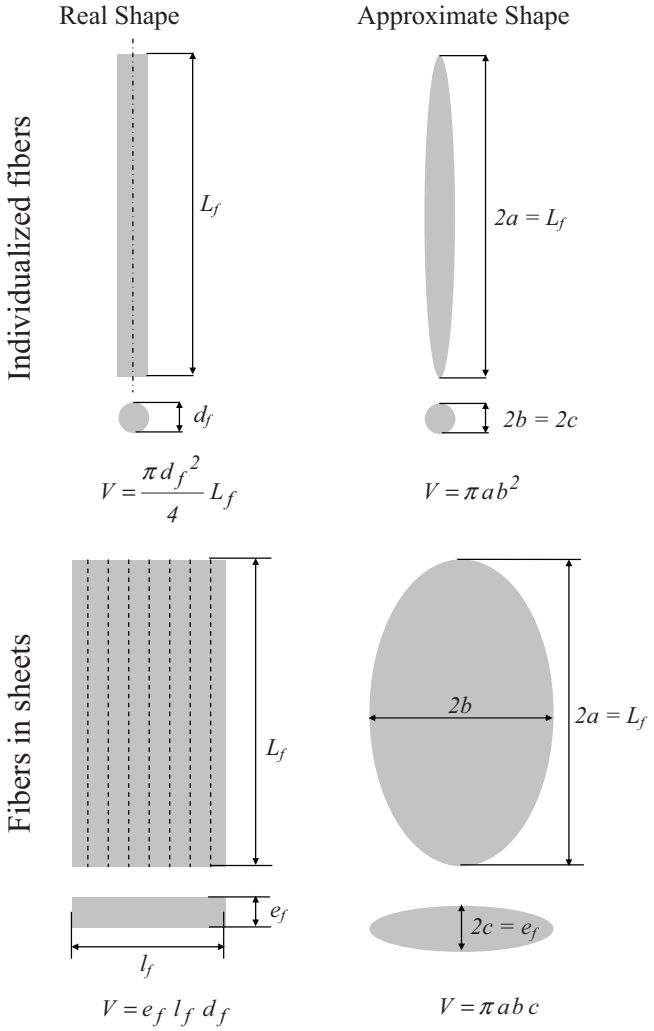

Fig. 1. Fibers geometry.

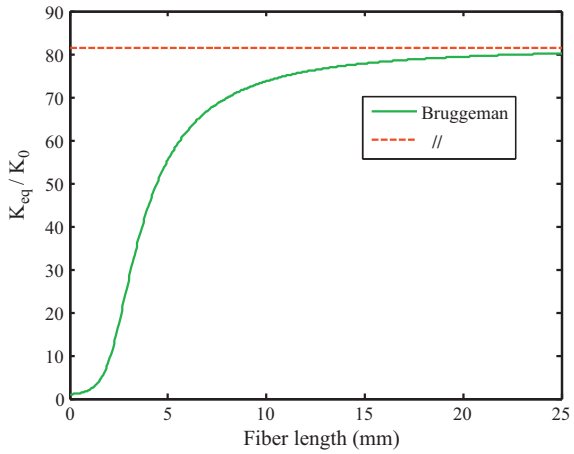

Fig. 2. Influence of the fibers length L_f on the permeability for constant values $\varepsilon_f = 0.34$ and $d_f = 15$ μm.

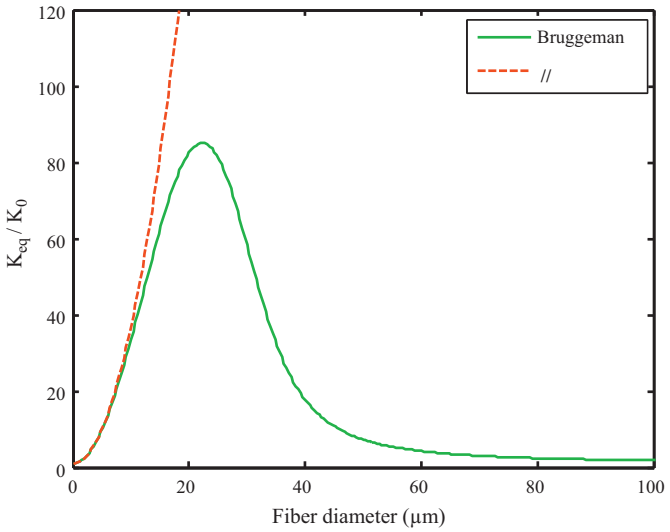

Fig. 3. Influence of the fibers diameter d_f on the permeability for constant values $\varepsilon_f = 0.34$ and $L_f = 10$ mm.

permeability ratio increases with the fibers length L_f from the value of the continuous phase K_0 obtained for moderate values of the ratio d_f/L_f. Decreasing the ratio d_f/L_f, A_0 (which is only a function of d_f/L_f) tends towards 0 and, in the case $\varepsilon_1 << 1$ and the permeability K_{eq} tends asymptotically towards the limit for parallel fibers arrangement $K_{//} = (1 - \varepsilon_1/3)K_0 + (\varepsilon_1/3)K_1$ assuming that one-third of the hole is directed in each orthogonal space direction. Qualitatively, this behavior is in agreement with the experimental results of Pandolfelli and co workers [5–8] who experimentally gives an optimal length around 6 mm while the theory shows that for a length $L_f = 10$ mm the permeability is 10% lower than the asymptotic limit $K_{//}$.

Fig. 3 represents the influence of the fibers diameter d_f on the equivalent permeability for a fiber length $L_f = 6$ mm and for the same fibers volume fraction $\varepsilon_f = 0.34$ %. On one hand, fibers with small diameter have a low longitudinal permeability K_f. On the other hand, when the fiber diameter increases, their number decreases. Therefore, Fig. 3 shows the existence of an optimal diameter in the range $20 < d_f < 30$ μm.

3. Material and methods

3.1. Castable preparation

Considering the great diversity of commercialized concretes, three types are chosen: two low-cement concrete (Castable A et C) and an ultra low cement concrete (Castable B). The main characteristics of these concretes are listed in Table 1.

The concrete was spoiled with a precise percentage of water, as recommended by the manufacturer (Table 1). Water + - concrete were mixed quite a long time to get the mixture homogeneous and with the right consistency. The optimal mixing time is 5 min. The mixture is then cast in standard bricks (230 mm × 114 mm × 63 mm) which are cut to obtain cylinders of diameter and height 50 mm for the permeability measurement. Once cast, the bricks have been stored at15 °C, wrapped in a plastic bag during 24 h (curing time).

The polypropylene fibers are of two types: individualized fibers or precut sheets as shown on Fig. 1. At the beginning of this study, a first question was to know if the concrete mixing can separate these sheets in individualized fibers. In order to apply the Bruggeman model, fibers sheets are approximated by ellipsoids with $2a = L_f$, $2c = e_f$ where e_f is the thickness of the sheet and $2b$ is calculated such as the volume of the ellipsoid is preserved (Fig. 1).

3.2. Experimental procedure

3.2.1. Experimental device

The measuring device is a confinement cell with input pressures up to 10 bars (Fig. 4). The sealing of the sample is ensured by a flexible silicone membrane inflated to about

Table 1
Characteristics of studied concretes.

	Base	Al_2O_3 content	Cement content	Water mixing
Castable A	Tabular alumina reactive alumina (fine particles)	98 wt.%	5 wt.%	5.25 wt.%
Castable B	Bauxite micro silica (fine particles) polymeric fibers	85 wt.%	2 wt.%	4 wt.%
Castable C	Andalousite, chamotte, kerphalite, other raw materials micro silica (fine particles) polymeric fibers	60 wt.%	6 wt.%	6.1 wt.%

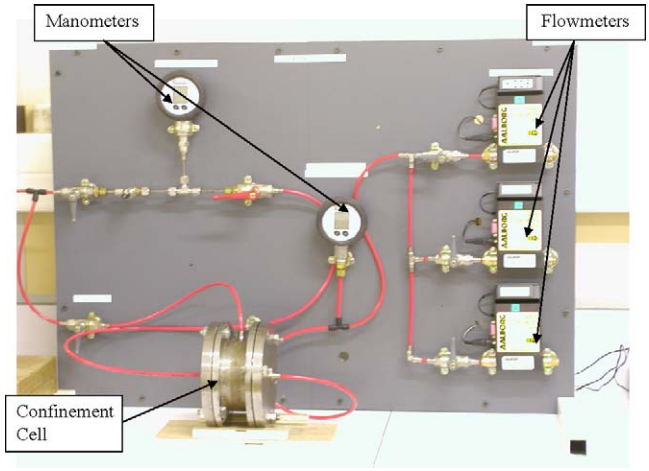

Fig. 4. Overview of the gas permeability measuring device.

15 bars as counter-pressure. A gauge covering the range from 0 to 20 bars measures the input upstream pressure. The pressure inside the sample cannot of course exceed the counter-pressure. At the output, the downstream pressure and the volumetric gas flow are measured. The measuring range of flow can vary from 0 to 200 ml min^{-1} using three different flowmeters. This device allows the permeability measurement down to 10^{-18} m^2 using an upstream pressure of 4 bars and a volumetric flow of 0.15 ml min^{-1} (minimum measurable volume flow).

3.2.2. Method

A constant pressure drop is applied between the top and the bottom of the sample of length ΔL. The inlet pressure P_i, the outlet pressure P_o and the volumetric output flow q_w are measured when the steady state is reached. The equivalent permeability is measured according to the classical relation:

$$K = \frac{2P_o \Delta L q_o}{P_i^2 - P_o^2} \tag{18}$$

with

$$K = K_{liq}\left(1 + \frac{B}{(P_i + P_o)/2}\right) \tag{19}$$

if the Klinkenberg effect has to be taken into account. In order to test the pressure effect on the permeability, a series of experiments was conducted to collect a large amount of data on the permeability of the studied materials. The three tested concretes exhibit different levels of permeability and, therefore, with specific behaviors.

To identify the influence of the presence of fibers on the permeability, tests are conducted after firing at different temperatures: 80, 120, 160, 200 and 400 °C. The firing is stopped when the sample mass does not vary anymore. The experiment consists in measuring the permeability of a refractory concrete using the device described above varying the proportion of fibers. Castable C with different quantities of fibers added (ω_f = 0; 0.05; 0.1 and 0.2 wt.%) was used for the experiments. The fibers are added during the mixing occurring in two stages: first concrete and fibers are mixed during around 5 min to disperse the fibers; then water (6.1 wt.%) is added and the final mixing lasts again 5 min. The mixture is then cast in standard bricks (230 × 114 × 63 mm^3) which are cut to obtain cylinders of diameter and height 50 mm for the permeability measurement.

4. Results and discussion

4.1. Pressure effect

Considering a concrete sample of thickness 50 mm, porosity 10% submitted to a pressure drop of 10 bars, the condition Re > 1 for the consideration of the inertial effects is verified only for permeabilities over 10^{-14} m^2.

Applying Jones correlation (4) and considering a pressure P = 2 bars, the corrective term B/P of the Klinkenberg relation is higher than 0.1 when the permeability is lower than 10^{-14} m^2.

The permeability of the studied concretes is always lower than 3×10^{-15} m^2. Therefore only the Klinkenberg effect exists and must be taken into account for the interpretation of the permeability experimental measurements (no Forchheimer effect is possible).

Measurements at several pressure levels for the same sample are shown on a graph K versus $1/P_{av}$ where $P_{av} = (P_i + P_o)/2$. If the permeability follows Klinkenberg relation (3), a straight line of slope B and for the value at the origin K_{liq} is obtained. As shown in Fig. 5, all graphs K versus $1/P_{av}$ for the three tested concrete exhibit this type of behavior.

As shown in Fig. 5, the Klinkenberg effect is important and cannot be neglected. Table 2 gives a summary of the results obtained for the three tested concretes. A comparison of the Klinkenberg coefficient B-values between experimental determination and Jones correlation (4) is shown: the B-values are in agreement with the order of magnitude given by Jones' correlation.

4.2. Fiber effect

4.2.1. Experience

The effect of fibers was experimentally studied by measuring the permeability of concrete C samples without fibers and with fiber mass fractions ω_f = 0.05%; 0.1% and 0.2%. Due to the small values of the samples permeability (10^{-16} m^2), the Klinkenberg effect is important and a correction of the experimental values is needed. This is the main difference with the results of Pandolfelli and co workers [2–4,6]. As the range of investigated pressure is small, it would be difficult to determine simultaneously K_{liq} and b according to Eq. (19) from a linear regression K versus $1/P_{av}$ with a satisfying accuracy. Therefore, the permeability values are interpolated at a reference gas pressure P_{ref} = 2 bars.

Fig. 6 shows the permeability evolution for various firing temperatures between 80 °C and 500 °C and for four mass fractions of polypropylene fibers (ω_f = 0; 0.05; 0.10; 0.20 wt.%). First note that the permeability of the material without fibers (black curve) represented on a logarithmic scale

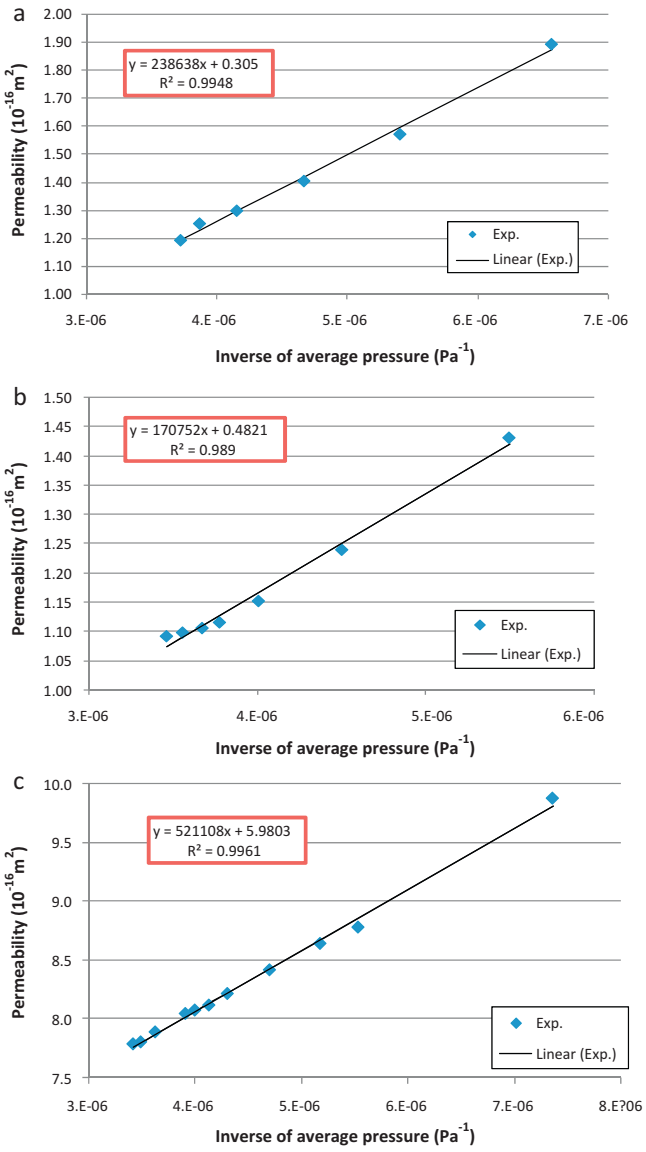

Fig. 5. Permeability versus the inverse of the average pressure $1/P_{av}$ for different materials: (a) castable A, (b) castable B and (c) castable C.

increases steadily with the firing temperature. The temperature rise promotes the shrinkage of the cement-related phase linked to physico-chemical transformations as hydrates dissociation, as studied by Schmitt et al. [19]. Adding polypropylene fibers leads to an additional increase of the permeability except perhaps for the case 0.05 wt.% (red curve). The curves for 0.10 wt.% (green curve) and 0.20 wt.% (blue curve) fibers amount exhibit a strong increase between 120 and 180 °C linked to the melting of the fibers.

Table 2
Liquid permeability of concretes and Klinkenberg's coefficient.

Material	K_{liq} (m^2)	b (bar)	b_{Jones} (bar)
Castable A	3.05×10^{-17}	7.83	1.67
Castable B	4.82×10^{-17}	3.54	1.41
Castable C	9.98×10^{-16}	8.71	5.71

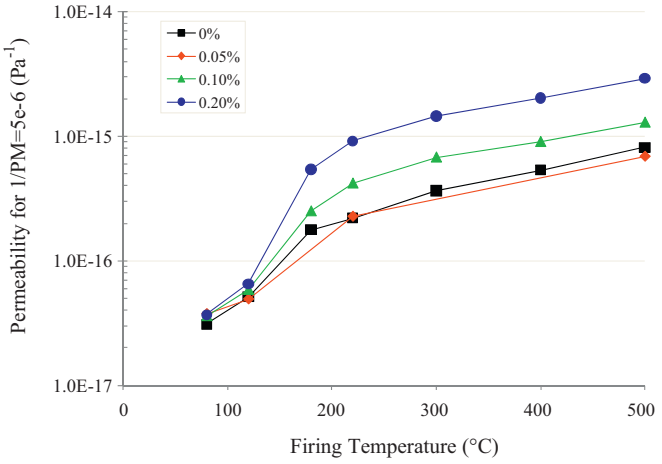

Fig. 6. Permeability variation with the firing temperature and (wt.%) fiber proportion.

To analyze the two effects (physico-chemical transformations and fibers melting) separately, Fig. 7 compares the temperature evolution of the permeability reduced by the permeability value at the same temperature but without fibers. This representation highlights the effect of fibers on permeability. For 80 °C and 120 °C, fibers do not change significantly the permeability. Between 120 °C and 220 °C, the increase corresponding to the fibers melting is clearly seen. For the concrete with 0.1 wt.% fibers, the ratio increases approximately from 1 to 2, while for the concrete with 0.2 wt.% fibers, the maximum value exceeds 4 when all the polypropylene fibers are melted. Beyond 220 °C, the ratio K_{eq}/K_0 is rather constant. This result is in agreement with the developed model leading to relation (17) showing that, for the considered values of the permeability, the ratio K_{eq}/K_0 does not depend on the permeability K_0.

After experimentally showing the influence of polypropylene fibers on the permeability, the next step is to compare these experimental results with the theoretical results of Bruggeman model predictions.

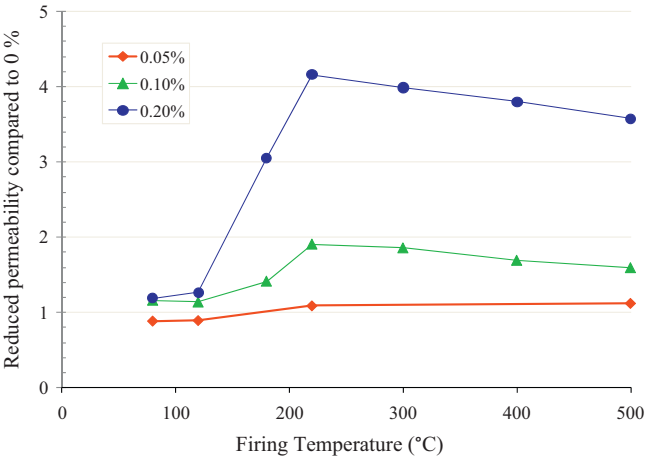

Fig. 7. Variation of the reduced (compared to 0% fibers) concrete permeability with the firing temperature.

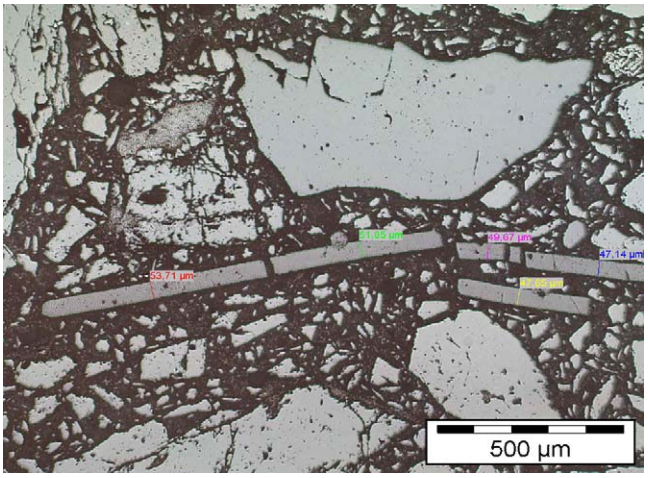

Fig. 8. Microscopic view of fibers located in the concrete (magnification: 50×).

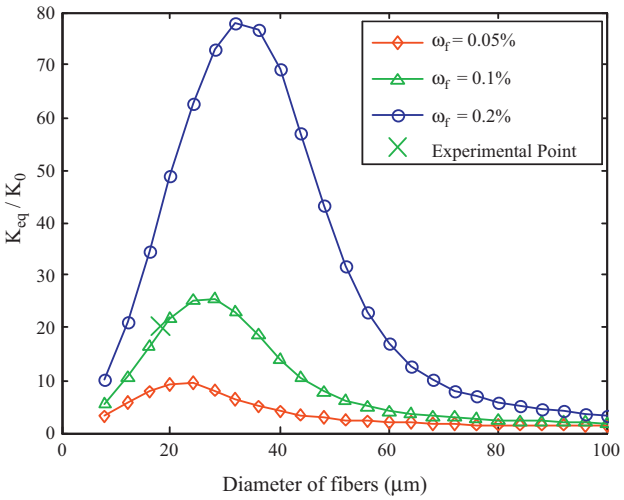

Fig. 10. Influence of the fibers diameter on the permeability gain compared with experimental results.

4.2.2. Modeling

To apply Bruggeman model to the experimental results, it is necessary to estimate the fibers dimensions. According to the manufacturer description, the fibers are in the form of sheets of length $L_f = 2a = 6$ mm, width $l_f = 2b = 0.5$ mm and thickness $e_f = 2c = 50$ µm. The rectangles that appear in the microscopic views of Fig. 8 have all the same width (around 50 mm). They may be interpreted as cross-section of sheet shape fibers considered as rectangle parallelepipeds with dimensions $500 \times 50 \times 6000$ mm (as given by the manufacturer). The different lengths of these rectangles may be explained by the different angles between the section plane and the fibers. The analysis of these microscopic views also leads to validate the hypothesis of a relatively good homogeneity of the matrix: at the scale of the length of fibers, the mixture aggregates + binding phase can be considered as a homogeneous medium of permeability K_0.

Fig. 9 shows the equivalent permeability given by the Bruggeman model assuming that the fibers are not individualized but in the form of sheets. The theoretical values of the ratio K_{eq}/K_0 depend *a priori* not only of the holes geometry (through the parameter A_0) but also slightly of the ratio K_1/K_0. In this case, the simplified relation Eq. (17) gives the same result as the Bruggeman model Eq. (15). Therefore the curves drawn on Fig. 9 are independent of the matrix permeability K_0. The experimental points are also plotted on Fig. 9, using the sheet dimensions given by the manufacturer. The theoretical prediction of the model is in good agreement with the experimental results.

The manufacturer sells another quality of fibers already individualized. The experimental results obtained with $\omega_f = 0.1$ wt.% for these individualized fibers are shown in Fig. 10 and compared with the prediction given by the Bruggeman model. Again, the experimental results agree with those predicted by the model. Therefore the model could be used as a tool to optimize the fibers amount and geometry.

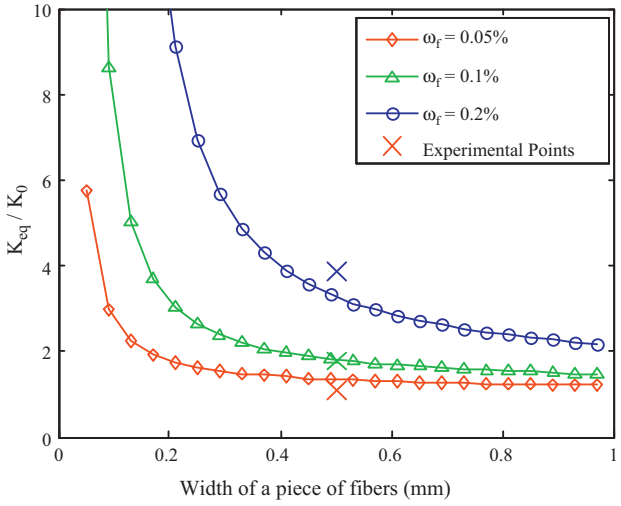

Fig. 9. Influence of the sheet width on the permeability gain compared with experimental results.

4.3. Temperature effect

Fig. 11 shows the evolution of the reduced permeability by the value obtained at 80 °C for various firing temperatures. The

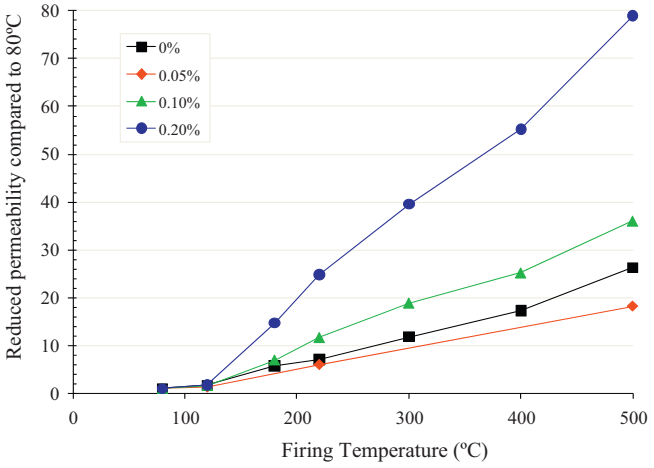

Fig. 11. Variation of the reduced permeability by the value at 80 °C with the firing temperature.

figure shows the simultaneous firing temperature and fibers effect on the permeability of the tested concretes. The permeability increase due to the temperature alone can be easily seen on the curve for the concrete without fibers. The permeability between 80 and 500 °C is multiplied by a factor of this order of 25. The maximum fibers effect for ω_f=0.20 wt.% and for the same temperature range is only of the order of 3.5. The temperature is therefore much more influent than the fibers disappearance on the permeability. This is not surprising because the concrete C used includes a big proportion of green raw materials which, as temperature increases, facilitates residual shrinkage within the microstructure.

5. Conclusion

As dense refractory castables have low permeability, Klinkenberg effects are important and must be taken into account in the permeability measurement. The influence of adding organic polypropylene fibers on the permeability has also been investigated varying both temperature and fibers amount. The temperature effect on permeability increase is found to be significant, especially with concrete containing green raw materials. Fibers inclusion has no effect on permeability until the fibers melt between 120 °C and 220 °C. Above 220 °C, there is no more fibers effect on the permeability. Knowing the fiber geometry, Bruggeman model leads to a very satisfactory prediction of the permeability increase due to the fibers.

References

[1] Z.P. Bazant, W. Thonghutai, Pore pressure and drying of concrete at high temperature, ASCE J. Eng. Mech. (EM5) (1978) 1059–1079.
[2] M.D.M. Innocenti, A.R.F. Pado, V.R. Salvini, V.C. Pandolfelli, How accurate is Darcy's law for refractories, Am. Ceram. Soc. Bull. 78 (11) (1999) 64–68.
[3] M.D.M. Innocenti, V.R. Salvini, V.C. Pandolfelli, J.R. Coury, Assessment of Forchheimer's equation to predict the permeability of ceramic foams, J. Am. Ceram. Soc. 82 (7) (1999) 1945–1949.
[4] M.D.M. Innocenti, V.C. Pandolfelli, Permeability of porous ceramics considering the Klinkenberg and the inertial effects, J. Am. Ceram. Soc. 82 (7) (1999) 1945–1949.
[5] R. Salomão, C.S. Isaac, F.A. Cardoso, M.D.M. Innocenti, V.C. Pandolfelli, PSD polymeric fibers and the permeability of refractory castables, Am. Ceram. Soc. Bull. 83 (10) (2003) 931–935.
[6] R. Salomão, F.A. Cardoso, M.D.M. Innocenti, V.C. Pandolfelli, Effect of polymeric fibers on refractory castable permeability, Am. Ceram. Soc. Bull. 82 (4) (2003) 51–56.
[7] R. Salomão, A.M. Zambon, V.C. Pandolfelli, Polymeric fiber geometry affects refractory castable permeability, Am. Ceram. Soc. Bull. 85 (4) (2006) 9201–9205.
[8] R. Salomão, V.C. Pandolfelli, Polypropylene fibers and their effect on processing refractory castables, Int. J. Appl. Ceram. Technol. 4 (6) (2007) 496–502.
[9] R.B. Bird, W.E. Stewart, E.N. Lightfoot, Transport Phenomena, Wiley, New York, 1960.
[10] S. Ergun, Flow through packed columns, Chem. Eng. Prog. 48 (2) (1952) 84–88.
[11] D. Ruth, H. Ma, On the deviation of the Forchheimer equation by means of averaging theorem, Transport Porous Med 7 (1992) 255–264.
[12] L.J. Klinkenberg, The Permeability of Porous Media to Liquid and Gases Drilling and Production Practice, American Petroleum Institute, 1941, pp. 200–213.
[13] W. Tanikawa, T. Shimamoto, Klinkenberg effect for gas permeability and its comparison to water permeability for porous sedimentary rocks, Hydrol. Earth Syst. Sci. Discuss. 3 (2006) 1315–1338.
[14] S.C. Jones, M. Aime, A rapid accurate unsteady-state Klinkenberg permeameter, Soc. Petrol. Eng. J. 12 (5) (1972) 383–397.
[15] D.A. De Vries, The thermal conductivity of granular materials, Bulletin de l'Institut National du Froid (1952) 115–131.
[16] S. Torquato, Random Heterogeneous Materials: Microstructure and Macroscopic Properties, Springer-Verlag, New York, 2002.
[17] H.S. Carslaw, J.C. Jaeger, Conduction of Heat in Solids, 2nd, Oxford University Press, 1959, pp. 427–428.
[18] R.W. Johnson, The Handbook of Fluid Dynamics, CRC Press, Springer, 1998, pp. 9.6–9.7.
[19] N. Schmitt, J.F. Hernandez, V. Lamour, Y. Berthaud, P. Meunier, J. Poirier, Coupling between kinetic of dehydration and physical and mechanical behaviour for high alumina castable, Cement Concrete Res. 30 (2000) 1597–1607.